Full Length Article

Design and performance analysis of a solar dual fluidized bed gasifier

M. Suárez-Almeida , A. Gómez-Barea , J. Salinero

Chemical and Environmental Engineering Department, Escuela Técnica Superior de Ingeniería, University of Seville, Camino de los Descubrimientos s/n, 41092 Seville, Spain

A B S T R A C T

The potential to conduct allothermal steam-gasification of biomass using a dual fluidized bed gasifier (DFBG) assisted by solar energy has already been conceptually proposed. In this paper the design and operation of a solar DFBG (SDFBG) device to deal with this concept is assessed by modeling, considering thermodynamic, kinetic and fluid-dynamic issues. The challenges identified in previous works, as well as the modifications required in the current state-of-the-art technologies of (no-solar) DFBG for implementing the new solution using heated particles as heat carriers, are worked out. Two SDFBGs, considering different arrangements for integrating the solids carrying the solar energy into the system, are designed. The operation of both under different solar-external heat loads, from autothermal operation (no external heat) to 3 MJ $kg_{bio,daf}^{-1}$ of external heat, is assessed and compared. This work shows how the technology can be implemented and scaled up.

1. Introduction

The use of solar energy as external heat source for steam reforming of fuels has been recognized as highly attractive method for increasing the share of renewable energy and reduction of CO_2 emissions [1,2]. Steam gasification of biomass and wastes is a highly endothermic process, producing high-quality syngas (N_2-free and high concentration of H_2) which can be further processed in catalytic reactors to produce renewable fuels and/or chemicals. Solar steam gasification of biomass is an attractive technology for generating solar biofuels with high share of renewable energy in storable form.

Although a great deal of solar gasifiers has been tested at laboratory scale [3,4], indirect solar gasification using a heat carrier [5,6] seems to be the only scalable approach enabling to decouple the operation of the gasifier from the intermittency of the solar radiation by an intermediate thermal energy storage [7].

A new concept of biomass gasification assisted by solar thermal energy, as an extension of a state-of-the-art (no-solar) dual fluidized bed gasification (DFBG), has been recently proposed by the authors [7,8]. The solid particles act as thermal energy carrier, circulating between the solar receiver and the gasifier with intermediate thermal energy storage. The main advantage of this configuration is that the solar receiver and the reactor are uncoupled, while thermal integration is highly efficient since carrier particles are directly used in the reactor.

In these previous studies [7,8] mass and energy balances were formulated to give insight on the main operating conditions: reactors and solar receiver temperatures, ranges of internal (gasifier-combustor) and external

(SDFBG-solar loop) solids circulations, as well as the maximum achievable char conversions and solar shares. These works also identified the main challenges for developing and scaling-up the process: the redesign of the gasification unit and the control of solids circulation to adapt the operation to changes in solar external heat load. The objective of this paper is to propose a design for the SDFBG enabling the requirements identified in previous studies, and to analyze the operation of the system. To cope with these objectives, a reactor model of a DFBG is developed considering both, thermochemical (including kinetics) and fluid dynamics aspects that were not considered in previous works. The performance of the concept taking into account the solar field and thermal energy storage were already analyzed [8] and is not considered in this study.

2. SDFBG concept

The conceptual integration of the solar gasification system is presented in Fig. 1(a) [8]. The solid particles acting as thermal energy carrier circulate between the solar side and the DFBG. Two tanks are used, the hot material storage (HMS), to store the particles heated in the solar receiver, and the warm material storage (WMS), to store the particles leaving the gasification system, allowing for temporary thermal storage of solar energy. The DFB gasification system, represented inside the dash-dotted line in Fig. 1(a) and detailed in Fig. 1(b), is composed of a gasifier (typically a bubbling FB) where the biomass is injected, devolatilized and the char is partially gasified with steam, and a combustor (typically a fast FB) where the char coming from the gasifier is burned with air. In this arrangement, the gasifier is heated by both the circulating hot material coming from the combustor and that from the

Nomenclature

A	cross section, m^2
a	decay coefficient, m^{-1}
c_p	specific heat of solid inert material, kJ kg^{-1} K^{-1}
d_{out}	cyclone exit duct diameter, m
d_p	particle size, m
E_∞	elutriation constant, kg m^{-2} s^{-1}
ER_{H2O}	steam equivalence ratio, -
F	mass flowrate, kg s^{-1}
F_{inert}	total flowrate of inert material leaving the gasifier, kg s^{-1}
F_s	flowrate of solids inert material, kg s^{-1}
g	gravitational acceleration, m/s^{-2}
G_s	solids flux of inert material (referred to riser cross section), kg m^{-2} s^{-1}
h	height, m
H_G	specific heat required by the gasifier, kJ kg$_{bio,daf}^{-1}$
$R_{C\text{-}H2O}$	reactivity of char steam gasification, s^{-1}
$R_{C\text{-}H2O,ref}$	reactivity of char steam gasification for the reference case, s^{-1}
n_i	molar yield of species i in the product gas (per mol of biomass), -
P	pressure, Pa
Q	gas flowrate, m^3/s
R_{LLS}	fraction of gas flowing through the recycle chamber, -
SEH	specific external (solar) heat, MJ kg$_{bio,daf}^{-1}$
T	temperature, °C
Th	biomass throughput (referred to the gasifier), kg h^{-1} m^{-2}
u_0	superficial velocity, m/s
u_{critic}	critic velocity defined as in Eq. (8), m/s
u_g	actual gas velocity, m/s
u_{mf}	minimum fluidization velocity, m/s
u_s	solids velocity, m/s
u_t	particle terminal velocity, m/s
W	solids inventory, kg
x_{char}	char conversion of a single particle, -
X_{char}	average char conversion in the gasifier, -
x_{O2}	molar fraction of O_2 in the riser fluidizing gas, -

Greek symbols

β	gas-particle interaction, kg m^{-3} s^{-1}
δ	bubble fraction, -
ΔP	pressure drop, Pa
ε	voidage, -
λ_{H2O}	steam to biomass molar ratio, -
λ_{O2}	oxygen to biomass molar ratio, -
μ_g	viscosity of the gas, kg m^{-1} s^{-1}
ξ	constant dependent on the cyclone geometry, -
ρ	density, kg m^{-3}
$\rho_{h=0}$	solids concentration at the top of riser dense zone, kg m^{-3}
τ_{char}	char residence time in the gasifier, s
φ	particle sphericity, -

Subscripts

bio	biomass
C	referred to the flowrate of solids coming from the combustor/combustor temperature
daf	dry basis ash free
dz	referred to the riser dense zone
g	referred to the gas
G	referred to the gasifier
in	referred to the cross section of the inlet of the cyclone
max	maximum
mf	minimum fluidization
out	referred to the cross section of the outlet of the cyclone
p	referred to the particle
s	solids
T	referred to total inventory of inert solids
top	referred to the top of the riser

Abbreviations

C1	referred to configuration 1 (according to Fig. 2)
C2	referred to configuration 2 (according to Fig. 2)
CFM	cold flow model
DC	down comer
DFB	dual fluidized bed
DFBG	dual fluidized bed gasifier
FB	fluidized bed
FBG	fluidized bed gasifier
HMS	hot material storage
LLS	lower loop seal
RC	recycle chamber
SC	supply chamber
SDFBG	solar dual fluidized bed gasifier
SEH	specific external heat
TDH	total disengagement height
ULS	upper loop seal
WGSR	water–gas-shift reaction
WMS	warm material storage

hot material storage (HMS). Different configurations for integrating the solar external solids into the system were analyzed in [8] but only Configuration 1 (C1) and Configuration 2 (C2), identified as the best options, are considered in this work (Fig. 2).

The SDFBG will operate with high share of external heat when solar energy is available (either from the solar receiver or from the HMS), while it will send more char to the combustor as the solar external heat decreases. The use of solar energy enables the increase in char conversion to syngas in the gasifier from 20% (typical in conventional DFBG, where the rest of the char must be burned in the combustor to thermally maintain the system) up to 80%, a reasonable limit calculated in [7,8] for SDFBG. As a result, more char need to be converted in the gasifier and the required inventory is increased up to ten times with respect to conventional designs of DFBG. Too large gasifier volume would be required for fully allothermal gasification, i.e., 100% char conversion in the gasifier.

Fig. 1(b) presents a sketch of the DFBG including its main parts. This design is conceived for the operation of the integrated solar gasification process both, at high allothermal conditions, i.e., high char conversion in the gasifier; and completely autothermal conditions, when there is neither solar nor thermal energy storage availability and all the energy for the gasification is obtained from the combustion of char. A wide bubbling FB gasifier (compared to conventional DFBG [9]) is required, to allow enough residence time for the char to be converted while keeping the maximum pressure drop of the gasifier under reasonable values [10]. The riser-combustor and the gasifier are joined by two loop seals: the upper loop seal (ULS) acting as a merely sealing and solids recirculation system, and the lower loop seal (LLS), which plays a key role in the operation of the system under different external heat loads. The length and width of the supply chamber (SC) of the LLS needs to be particularly designed for compensating the changes of pressure drop in the gasifier resulting from the variation of the solar external heat introduced into the system.

Furthermore, the integration of the solar solids into the system implies particular considerations when designing the SDFBG due to the different patterns of solids circulation as the solar external heat is increased: in Configuration 1 (C1, Fig. 2(a)) the solids flux from the riser
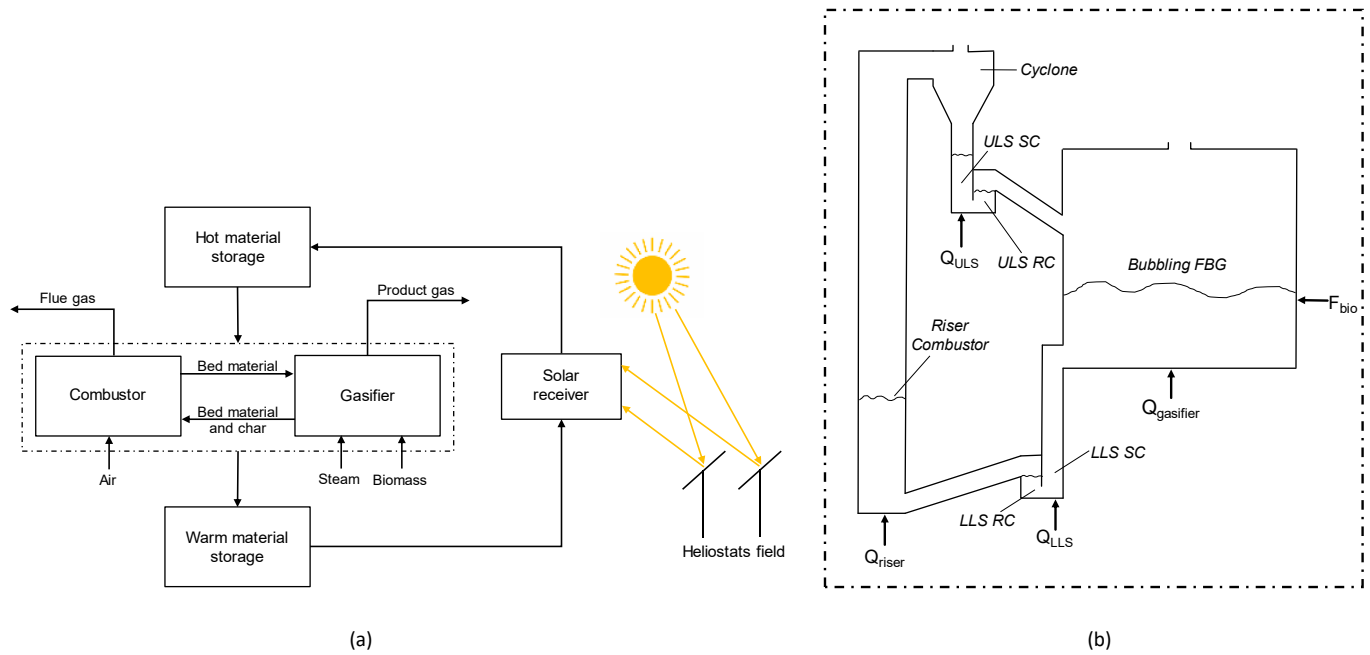
Fig. 1. SDFBG: (a) conceptual layout of the process; (b) sketch of the DFBG modeled (inlet and outlet of inert bed material are not represented).

highly decreases (lower heat is required from char combustion to sustain the gasification), while under Configuration 2 (C2, Fig. 2(b)), although the char conveyed to the combustor also decreases, the solids entrainment in the riser is rather constant since the solids from the external circulation are extracted from the combustor.

3. Modeling

The model considers the fuel-conversion units (fast fluidized riser and bubbling fluidized bed gasifier), a cyclone for separating the particles, and two loop seals, ULS and LLS, connecting the riser and the gasifier for the solids circulation. Steam is used as fluidizing agent in the gasifier and the loop seals and air/enriched air in the combustor (considering a single air entrance at the bottom of the unit). Fresh biomass is fed to the gasifier while unconverted char is burnt in the combustor [8]. External solids (circulating through the solar loop) are introduced/removed according to C1 or C2 in Fig. 2. The charging/discharging method and its implications in the hydrodynamics of the SDFBG is out of the scope of this work.

For given operating conditions (gasification and combustion temperatures, inlet temperatures of the fluidizing agents, biomass and solar solids, bed material properties, steam to biomass ratio, oxygen content of the riser fluidizing gas, solar external heat and pressure at the gasifier and combustor outlets) the model calculates the syngas composition and char conversion in the gasifier, the solids circulation (both internal and external), the gas flowrate required in the combustor, the total solids inventory and the pressures and solids distribution around the system.

The model of the SDFBG presented here is based on previous

separated thermochemical [8] and hydrodynamics [10] models. Both models are joined together here after some modifications (mainly regarding the fluid-dynamics of the loop seal and the riser). The main elements of the model emphasizing the new considerations are summarized in the following sections.

3.1. Thermochemical model

The steam gasification process (in the gasifier unit) of a typical wood biomass [11] is represented by

$$CH_{1.5}O_{0.7} + \lambda_{H_2O}H_2O \rightarrow n_{H_2}H_2 + n_{CO}CO + n_{CO_2}CO_2 + n_{CH_4}CH_4 + n_{C_2H_4}C_2H_4$$
$$+ n_{H_2O}H_2O + n_{C_{10}H_8}C_{10}H_8 + n_{C_{(S)}}C_{(s)} \quad \text{(R1)}$$

where for the sake of simplicity the biomass (moisture and ash free) is assumed to be $CH_{1.5}O_{0.7}$, char to be pure solid carbon $C_{(s)}$, the light hydrocarbons are lumped into ethylene (C_2H_4) and tars into naphthalene ($C_{10}H_8$).

The gasifier is modeled following the approach described in [12]. The process is simplified by decoupling primary and secondary conversion. The primary yields of devolatilization are methane, ethylene, tar and char. Then the char is gasified with steam, the light hydrocarbons reformed with steam and the tar converted by reforming/cracking into light volatiles. The composition of the outlet gas is obtained by applying the equilibrium of the water–gas-shift reaction (WGSR) to the compounds released after devolatilization, and considering the overall atomic mass and heat balance over the entire gasifier, while taking into account the unconverted fraction of hydrocarbons, tar and char.

Other assumptions for modeling the gasification reactor are: (i) conversion of gaseous species assuming perfect mixing of gases both, in the bed and freeboard, and first order kinetics, with average gas residence time of 1 s (the actual geometry of the reactor is not considered); (ii) char is removed from the gasifier with the solids circulating to the combustor (elutriation and mechanical removal of bottom ash are not considered) and (iii) the char is converted by steam gasification considering that the particles are perfectly mixed in the reactor and following the uniform conversion model.

The combustion unit has been modeled assuming instantaneous and complete conversion of the char [13], i.e. no unburnt char enters the gasifier with the solids coming from the combustor (nor coming from the
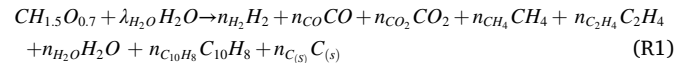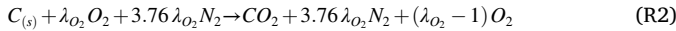

Fig. 2. Configurations for the integration of the solids heat carrier into the SDFBG system (dashed arrows represent the circulation from/to the solar loop; solid arrows defined as in Fig. 1(a)).

HMS under C2). The overall process in the combustor is given by

$$C_{(s)} + \lambda_{O_2}O_2 + 3.76\,\lambda_{O_2}N_2 \rightarrow CO_2 + 3.76\,\lambda_{O_2}N_2 + (\lambda_{O_2} - 1)\,O_2 \tag{R2}$$

The heat necessary for gasification (H_G) comes from the sensible heat of the solids coming from the combustor and from the HMS. For the sake of simplicity, the sensible heat of active particle, i.e., char, which represents a small fraction of the stream (<3% w/w), is neglected.

$$H_G = F_{s,C}\,c_p(T_C - T_G) + F_{s,HMS}\,c_p(T_{HMS} - T_G) \tag{1}$$

$F_{s,C}$ and $F_{s,HMS}$ are the flowrates of solids inert material coming from the combustor and from the HMS, respectively, into the gasifier. For a given solar external energy supplied to the system the model estimates the char that needs to be burnt in the combustor to balance the heat requirements in the gasifier as well as the corresponding average residence time of the char particles in the gasifier to completely convert the remaining char (that which is not circulated to the combustor). Note that, when it comes to estimate the char conversion in the gasifier, the concentration of char in the solids stream from the HMS in C1 is assumed to be equal to that of the gasifier, in agreement with the assumption of perfect mixing of solids (in C2 there is no char in the solids from the HMS). The accurate modeling of the SDFBG operation under C1 should consider the charge/discharge of the HMS/WMS over the time; i.e., taking into account the different degree of conversion of char particles in the storage over the time. This transient model is out of the scope of this work since it requires the specific design of the HMS and WMS units.

Further details of the model together with the kinetic expressions, equilibrium constant of the WGSR, biomass high heating value, devolatilization yields and heat capacity of the heat carrier employed in the model are reported in [8].

3.2. Fluid-dynamic model

The fluid-dynamic model rests on two conditions that are approximately fulfilled in any circulating fluidized bed: (i) the efficiency of the cyclone at the riser outlet is assumed to be unity therefore, for a given operating conditions, the mass inventory is constant within the system (Eq. (2)), and (ii) the difference of pressure between two points is equal to the pressure drops throughout the way between them (Eq. (3)). Moreover, the pressure drops across the openings in the loop seals, and that of the pipe connecting the ULS with the gasifier, together with the solids inventory in the cyclone are neglected.

$$W_T = W_{gasifier} + W_{LLS} + W_{riser} + W_{ULS} \tag{2}$$

$$\Delta P_{gasifier} + \Delta P_{SC,\,LLS} = \Delta P_{RC,\,LLS} + \Delta P_{riser} + \Delta P_{cyclone} \tag{3}$$

3.2.1. Gasifier

The inventory and pressure drop across the gasifier are given by Eq. (4) and (5) where the only unknowns are the height (h) of the bed and the voidage (ε) of the bubbling bed.

$$W = \rho_p(1 - \varepsilon)h A \tag{4}$$

$$\Delta P = \rho_p(1 - \varepsilon)h\,g \tag{5}$$

ε is calculated considering the bubble fraction (δ) and the porosity of the emulsion at minimum fluidization (ε_{mf}):

$$\varepsilon = \delta + (1 - \delta)\varepsilon_{mf} \tag{6}$$

The bubble fraction is estimated according to a model based on the modified two-phase theory [14] where the superficial velocity in the gasifier, is considered as the flowrate of the generated syngas (containing the steam fed through the bottom of the gasifier together with that flowing through the LLS SC and the gas generated from the biomass).

Note that the solids inventory in the gasifier is obtained from the

thermochemical model since it is linked to the required residence time for converting the char (τ_{char}) by Eq. (7), where F_{inert} is the total flowrate of inert material leaving the gasifier.

$$W_{gasifier} = \tau_{char}F_{inert} \tag{7}$$

3.2.2. Lower loop seal

The loop seal depicted in Fig. 3 consists of two chambers, supply chamber (SC) and recycle chamber (RC) divided by a baffle. Solids circulate downwards through the SC and upwards through the RC. A steam flowrate is fed to the loop seal through the SC (since it is the best option for promoting the circulation of gas through the SC) and divided between the two chambers. A sensitivity analysis to assess how different gas distributions in the LS affected the solids flux was made in [10]. The results showed that, unless the SC is fluidized, the solids flux is significantly affected by the gas division. However, the gas split and the solids flow behavior in a loop seal have been probed not to be easy to assess by simple 1D semi-empirical model. Detailed discussion is provided elsewhere [15,16].

In the present work some assumptions are made to assess by a simple model, the general performance and the role of the LLS within the new SDFBG concept. Since it is not possible to predict the gas split between the chambers of a loop seal by modeling, the gas velocity in the SC is set to meet the gas-solids relative velocity leading to the required pressure drop to satisfy the hydrodynamics at a given operating conditions while, the RC is assumed to operate always under incipient fluidization referred to solids flow (i.e., gas-solids relative velocity equal to minimum fluidization velocity). Moreover, the model neglects the pressure drop through the opening (between the SC and the RC). In the actual operation of a loop seal, the RC expands as more gas is fed to the SC [16], leading to a slightly lower solids inventory in the RC (compared to that of minimum fluidization) and a higher amount of steam circulated to the riser. However, the error introduced by these assumptions is not that to affect the conclusions of this study.

While the RC is always considered at minimum fluidization, the SC can operate as a moving bed or at incipient fluidization. For modeling purposes the voidage of minimum fluidization (ε_{mf}) is considered both for the operation under incipient fluidization and moving bed. Since the RC is always at incipient fluidization the pressure drop is given by the hydrostatic pressure (Eq. (5)), where the height is that of the weir; assumed constant during stable operation and given by the geometry (the height of the crest of solids is small compared to the weir height and therefore it is neglected).

The estimation of the pressure drop in the SC depends on the operating regime. There is a critical velocity defined in Eq. (8),
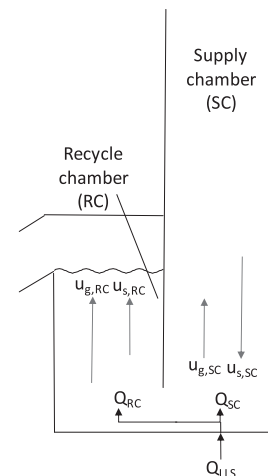

Fig. 3. Solids and gas velocities and fed gas distribution in the two chambers of the LLS.

comparing the relative superficial velocity with the minimum fluidization velocity: a positive critical velocity means that the SC is fluidized, while a negative means it is in moving bed regime. According to this premise, if the bed is fluidized the pressure drop is estimated from Eq. (5), while if it is under moving bed conditions it is estimated from Eq. (9), in both cases using the geometrical height of the SC.

$$u_{critic} = (u_{g,SC} + u_{s,SC}) \varepsilon_{mf} - u_{mf} \tag{8}$$

$$\Delta P = \frac{\beta}{\varepsilon_{mf}} (u_{g,SC} + u_{s,SC}) h \tag{9}$$

where

$$\beta = 150 \frac{(1 - \varepsilon_{mf})^2}{\varepsilon_{mf}} \frac{\mu_g}{\phi \, d_p^2} + 1.75 (1 - \varepsilon_{mf}) \frac{\rho_g}{\phi \, d_p} (u_{g,SC} + u_{s,SC}) \tag{10}$$

The solids inventory in the loop seal is estimated from Eq. (4), considering the geometry and height of each chamber.

3.2.3. Riser

The model of the riser has been simplified compared to that in [10]; a dense bottom bed and a transport zone are considered following the approach in [17]. Although this model provides a general understanding on the operation of the SDFBG a more dedicated model of the riser is required for a final design and scale-up of the process.

The dense bottom bed is modeled considering a constant mass fraction of solids equal to 0.2 [17]. The pressure drop and mass of solids in the dense zone are estimated according to Eqs. (4) and (5), where the height of the dense zone is not an input but calculated by the model.

The mean solids concentration along the transport zone is assumed to decay exponentially with height as described by the simplified model [17,18]:

$$\rho(h) = \rho_{TDH} + (\rho_{h=0} - \rho_{TDH}) \exp(-a \, h) \tag{11}$$

where $\rho_{h=0}$ is the solids concentration at the top of the dense zone, a is the decay coefficient, and ρ_{TDH} is the solids concentration at a height (h) higher than that at the total disengagement height (TDH), which is calculated according to Eq. (12). Note that the superficial velocity in the riser should consider not only the air fed to the riser (and gas coming from the char combustion) but also the gas flow through the recycle chamber of the LLS.

$$\rho_{TDH} = (1 - \varepsilon_{TDH}) \rho_p = \frac{E_\infty}{(u_0 - u_t)} \tag{12}$$

The solids density profile is estimated integrating Eq. (11) from the top of the dense bed to the top of the riser. If the momentum losses due to wall friction and solids acceleration can be neglected as compared with the static head of solids, the pressure drop is estimated according to Eq. (13).

$$\Delta P = g \int \rho(h) \, dh \tag{13}$$

The mass of solids is obtained from Eq. (14).

$$W = \frac{\Delta P A}{g} \tag{14}$$

The total pressure drop and solids mass inventory in the riser result from adding the pressure drop and solids inventory of the dense zone to those transport zone.

The solids flux circulating within the DFBG, G_s (kg m^{-2} s^{-1}), is

$$G_s = \rho_p (1 - \varepsilon_{top}) u_{s,top} \tag{15}$$

since the highly diluted region at the top of the riser allows assuming that the slip velocity equals the particle terminal velocity [17] and therefore, the solids velocity can be directly estimated as

$$u_{s,top} = \frac{u_0}{\varepsilon_{top}} - u_t \tag{16}$$

ε_{top} is the porosity at the outlet point of the riser (estimated from Eq. (11)).

3.2.4. Cyclone

The pressure drop across the cyclone is estimated using an empirical correlation, where the parameter ξ is mainly dependent on the cyclone geometry (see Table 1) and the gas velocity refers to that at the entrance of the cyclone [19],

$$\Delta P = \xi \rho_g \frac{u_0^2}{2} \tag{17}$$

3.2.5. Upper loop seal

Pressure drops and solids inventory in the ULS are estimated in the same form that for the LLS, however, an additional equation is needed since the height of solids in the SC/downcomer is given now by a pressure balance (and not from geometry). Considering both units opened to the same environment through the gas exit of the cyclone and the exit of the produced gas from the gasifier, the pressure balance equation is,

$$\Delta P_{SC,\,ULS} = \Delta P_{RC,\,ULS} \tag{18}$$

The ULS acts simply as a sealing and recirculating system, therefore, the steam flowrate fed to the ULS can be the minimum required for circulating the solids avoiding the gas leakage between units. Therefore, as it is not possible to estimate the gas split in the loop seal, it has been assumed the RC under incipient fluidization while the solids circulate through a stagnant gas in the SC.

3.3. Operating conditions

The operating conditions set for the study are summarized in Table 2. Temperatures and specific external heat (SEH, defined as the amount of heat coming from the HMS that is introduced per kilogram of dry-ash-free biomass) are selected, based on results from previous studies [7,8], looking for maximizing the char conversion in the gasifier while

Table 1
Summary of the fluid-dynamics model parameters.

Parameter		Value/Correlation	[Ref]
E_∞	elutriation constant	Colakyan & Levenspiel	[20]
ξ	constant dependent on cyclone geometry	$\xi = 16 \, A_{in}/d_{out}^2$	[21]
A_{in}/A_{riser}	cross sections ratio: cyclone inlet/riser	0.2 (assumed)	–
A_{in}/A_{out}	cross sections ratio: cyclone inlet/cyclone outlet	0.65 (assumed)	–
u_{mf}	minimum fluidization velocity	Grace	[22]
ε_{mf}	minimum fluidization voidage		
u_t	terminal velocity	Haider & Levenspiel	[23]
ε_{dz}	voidage of the dense zone in the riser	0.8	[17]
a	decay factor	$4/u_0$	[17]

Table 2
Operating conditions and inert particle properties.

Operating conditions		
Biomass throughput, Th	$kg_{bio,daf}\ h^{-1}\ m_{gasifier}^{-2}$	150
Gasifier temperature, T_G	°C	850
Combustor temperature, T_C	°C	905–864
HMS temperature, T_{HMS}	°C	950
Steam temperature	°C	500
Air temperature	°C	25
Steam equivalence ratio, ER_{H2O}[1]	–	2
Oxygen in the riser fluidizing agent, x_{O2}	v/v	0.21–0.3
Specific external (solar) heat, SEH	$MJ/kg_{bio,daf}$	0–3
Pressure of operation	Pa	101 325
Sand particles properties		
density, ρ_p	kg/m^3	2500
mean particle size, d_p	μm	200
sphericity, ϕ	–	0.87

[1] steam fed into the gasifier over that required to stoichiometrically convert the biomass into syngas (H_2 and CO).

keeping the solids circulation and the gasifier volume under reasonable values. The steam equivalence ratio was selected to promote the tar conversion without decreasing too much the efficiency of the process [24,25]. The particle size is selected to allow the operation of the gasifier as a bubbling fluidized bed and the riser as a fast fluidized bed, and circulating the required solids flux while keeping the maximum riser velocity under moderate values avoiding attrition and erosion problems [26,27].

4. Results and discussion

4.1. SDFBG design

The SDFBG needs to be dedicatedly designed to allow the operation at a wide range of solar external heat loads. The main challenge is the design of a gasification unit that enables the operation under conventional autothermal mode (char conversion below 30%) and high allothermal mode (char conversion close to 80%). This operation leads to huge changes in the solids inventory of the gasifier which directly impacts on the hydrodynamics of the system. An option allowing the gasifier to operate with lower changes in solids inventory is to modify the gasification temperature as the SEH is changed (i.e., decreasing the temperature as the SEH decreases, see Section 4.3.2 for details). However, the gasification temperature is the most influence variable over many key phenomena, such as tar generation and other gas–gas reactions so, keeping this temperature constant leads to a more controlled and safer operation, resulting in more uniform and steady syngas composition. Moreover, although a design with a single gasification stage (as that from the current conventional DFBG) has been adopted, several stages for the gasification unit can be conceived in future designs.

A special design and operation of the DFBG is required to satisfy the hydrodynamics of the unit, adapting the solids circulation to fulfill the thermochemical requirement under the wide range of external heat loads. Moreover, the integration of the external solids into the system (Fig. 2) leads to different patterns of solids circulation, requiring different designs of the SDFBG. The key parameter to be adjusted is the biomass that the SDFBG can process per unit of cross section of the gasifier to fulfil the requirements, i.e., the biomass throughput (kg h^{-1} m$_{gasifier}^{-2}$).

The design of the SDFBG is made under these considerations:

1. A range of specific external heat supplied to the system (SEH) desired for the operation of the SDFBG.

2. A maximum pressure drop in the gasifier, that for the operation at the highest SEH (maximum residence time of the char, i.e., mass inventory in the gasifier).
3. A reference for the maximum superficial gas velocity in the riser-combustor (considering a reference excess of air) for the auto-thermal operation, i.e., that requiring the highest amount of air for char combustion.
4. A LLS SC cross section to allow the operation under moving bed regime for the full range of SEH.
5. A LLS SC length able to give a hydrostatic pressure drop (at minimum fluidization conditions) equal to the difference of the gasifier pressure drops operating under the highest SEH and autothermal conditions.
6. A riser height able to entrain the required flow of solids under the full range of SEH.

The geometric relations for a SDFBG of 150 kg h^{-1} m$_{gasifier}^{-2}$ for both configurations of the external solids circulation indicated in Fig. 2, is presented in Table 3. The ULS SC cross section can be selected to guarantee the operation under fluidized flow (considering the solids flowing against a stagnant gas) for all the SEH range, provided that the ULS is considered just as a solids recirculation device. The cross section of the RC both, in the ULS and the LLS, is assumed equal to that of the SC in each unit (although it could be optimized for minimizing the requirement of gas, is out of the scope of this study) with a height leading to a pressure drop of 15 mbar (as a conservative value to absorb pressure fluctuations). How the values in Table 3 are selected taken the items 1–6 to satisfy the operating requirements is subjected to intellectual property [28] and is not discussed here. However, the performance analysis of the gasifier is included in the following Section, showing that both designs fulfil the previously discussed requirements. The design results in a wide gasification unit (compared to that of the conventional DFBG) to allocate the huge inventory required at high allothermal conditions and, a dedicated LLS to absorb the changes of pressure drop of the gasification unit when varying the SEH. In that way, modifying the gas-solids relative velocities in the supply chamber of the LLS (by the loop seal aeration and solids circulation), the pressure drop throughout the system is rather constant independently of the solids inventory in the gasification unit, allowing the operation of the system under the full range of SEH.

4.2. Performance analysis

The performance of the previously designed SDFBGs for processing 150 kg h^{-1} (considering a gasifier cross section of 1 m^2) is analyzed for the operating conditions of Table 2. The change in the main operating parameters is analyzed over the full range of SEH allowing the operation of the gasification unit with a pressure drop below or equal to 200 mbar.

The differences when operating and designing a SDFBG under configurations C1 and C2 arise since the internal circulations of solids (between the gasification and combustion units) follows different patterns. As shown in Fig. 4(a), in C1 the circulation of solids decreases as SEH increases, due to the lower requirement of heat in the gasification

Table 3
Geometry proposed for the SDFBGs processing a biomass throughput of 150 kg h^{-1} m$_{gasifier}^{-2}$ under C1 and C2 according to Fig. 2 (all variables are converted into actual numbers once $A_{gasifier}$ is defined).

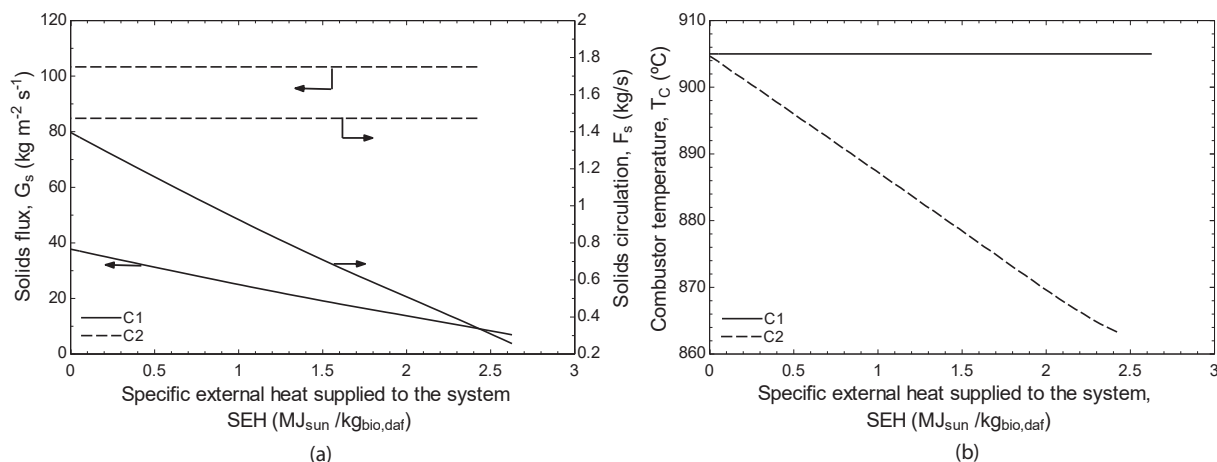|	C1	C2
$A_{riser}/A_{gasifier}$	0.037	0.014
$A_{SC,LLS}/A_{riser}$	0.505	3.382
$A_{RC,LLS}/A_{SC,LLS}$	1	1
$A_{SC,ULS}/A_{SC,LLS}$	1/2	1/2
$A_{RC,ULS}/A_{RC,LLS}$	1/2	1/2
$h_{SC,LLS}$ (m)	1.38	1.16
h_{riser} (m)	7.5	7.5

Fig. 4. Riser solids flux and solids circulation (a) and combustor temperature (b) against the SEH in SDFBGs for C1 and C2 (Fig. 2) and operating conditions of Table 2.

unit, as more heat comes from the external energy supply. On the contrary, in C2 the operation is carried out under constant circulation of solids while changing the combustor temperature (Fig. 4(b)). The latter operation is convenient for C2 since at any SEH the solids circulation through the combustor is considerable (solids from the external energy supply are continuously circulated through the combustor) but the amount of char decreases as the SEH increases. Therefore, operating the combustor at a constant temperature would limit the char conversion in the gasifier to that required in the combustor to rise the temperature of the circulating solids to the combustor temperature [8]. The internal solids circulation tends to the same value for the autothermal operation although, that from C2 is still slightly higher since at SEH=0 the char conversion achieved in the gasifier is higher (Fig. 5(a)) resulting in higher heat demand in the gasification unit.

The increase in the char conversion in the gasifier, resulting from the lower demand of heat from char combustion as more external energy is supplied to the system, is presented in Fig. 5(a). The maximum char conversion achieved is 79 and 75% under C1 and C2, respectively. Increasing the char conversion (i.e., the char residence time) beyond this point would violate the pressure drop restriction assumed in the gasification unit. It is shown that under C2 the conversion of char is considerably higher at low SEH where the losses by the sensible heat of the flue gases is lower due to the use of both, enriched air and lower oxygen excess ratio (at high SEH air with similar excess ratio is used in both

systems, resulting in a very close char conversion, Fig. 6(b-c)). This higher char conversion at low SEH leads to a syngas with a slightly higher concentration of CO (by reducing the CO_2 and H_2O content) under C2, Fig. 5(b). Furthermore, the increase in char conversion with increasing the SEH, leads to an increase of around 7% in the CO molar fraction, and a decrease of 8 and 5% in the H_2O and CO_2 molar fractions respectively, while H_2 and CH_4 are barely affected.

The gas flowrate through the riser is a key variable in the process since it has to fulfill both, the availability of oxygen to completely burnt the char in the combustor (oxygen excess ratio above 1) and the entrainment of the required solids circulation (which relates the gas velocity with the solids inventory in the riser). Consequently, at high SEH, the increase in the solids inventory in the system (and thus in the riser), as a result of the higher residence time required for converting the char in the gasifier together with the low circulation of char to the combustor, leads to a lower superficial gas velocity in the riser (Fig. 6(a)).

As shown in the previous section, a SDFBG requires from a narrower riser-combustor when operating under C2. The reason is that, under C2, the internal solids circulation is constant, but the char content decreases as SEH is increased. Therefore, the use of a wider riser (as that from C1) would lead to a huge oxygen excess ratio in the operation at high SEH, which requires from high solids entrainment but almost no char combustion (under C1 both, the char content and the solids entrainment, are low at high SEH). The operation at very high oxygen excess ratio is not
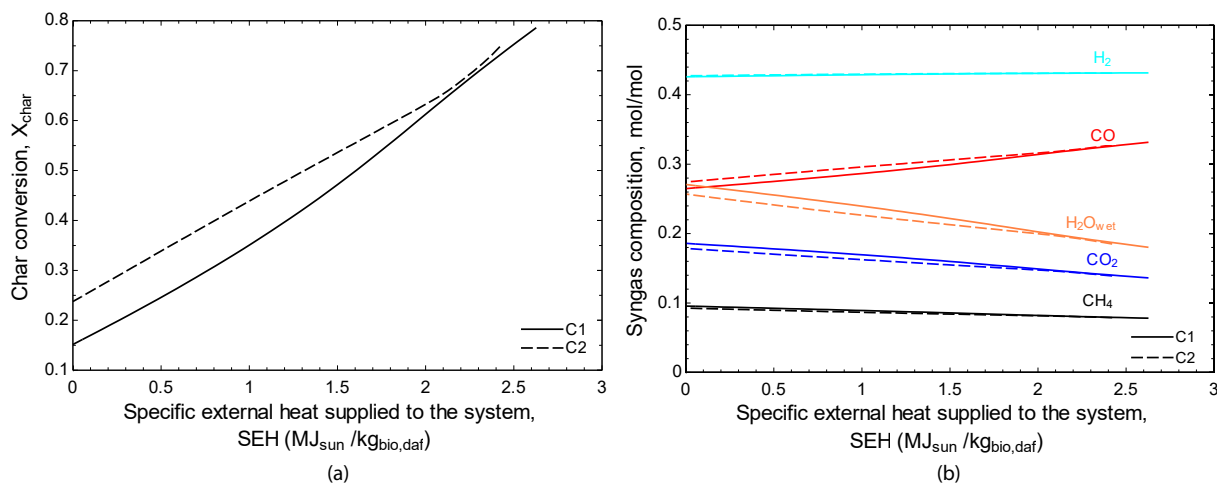

Fig. 5. Char conversion in the gasifier (a) and molar composition of the dry syngas (except to H_2O, which refers to wet gas) (b) as a function of the SEH in SDFBGs for C1 and C2 (Fig. 2), and operating conditions of Table 2.
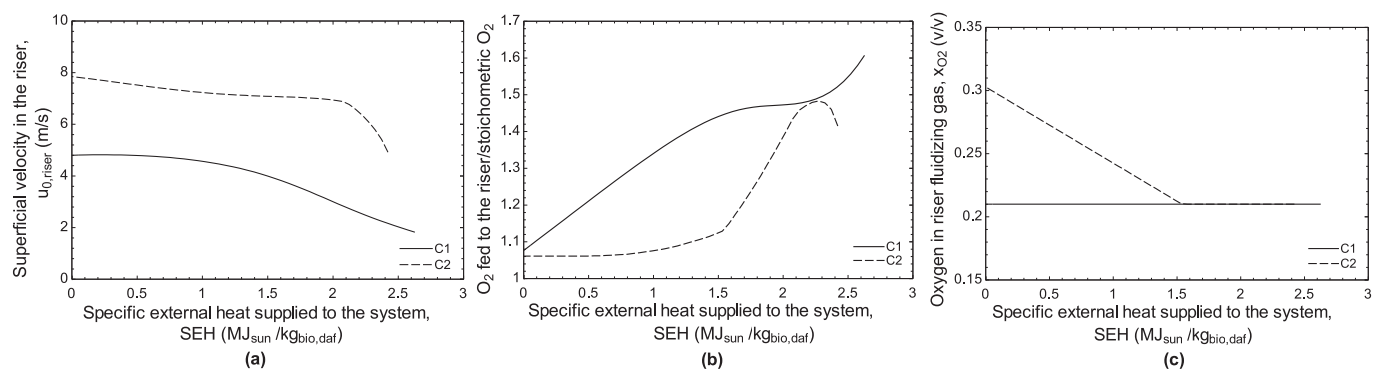
Fig. 6. Superficial velocity in the riser (a), oxygen fed to the riser compared to that stoichiometrically needed (b) and oxygen content of riser fluidizing gas (air/enriched air) (c), as a function of SEH in SDFBGs for C1 and C2 (Fig. 2) and operating conditions of Table 2.

convenient since it increases the sensible heat losses with the flue gas. Therefore, the adopted solution was to reduce the cross section of the riser to accomplish the required solids circulation at high SEH under lower oxygen excess ratios resulting in those of Fig. 6(b). The opposite behavior is found in the low range of SEH, where enriched air is needed to satisfy the char oxygen demand without an excess of solids entrainment (Fig. 6(c)).

The total solids inventory in the DFBG system must be adapted according to the external heat load (Fig. 7(a)): as the SEH in the system is increased, a higher residence time in the gasifier is needed to increase the char conversion. For a given SEH, higher solids inventory is required for the operation under C2 (Fig. 7(a)) due to: the higher char conversion at low SEH (compared to C1, Fig. 5(a)) and, at high SEH, the higher total flowrate of inert material leaving the gasifier (see Eq. (7)) resulting from the lower driving force of temperature of the external solids and those leaving the DFBG unit (T_{HMS}-T_C), compared to that of C1 (T_{HMS}-T_G). Therefore, for a maximum pressure drop in the gasifier, the external heat load that can be introduced in C1 (SEH=2.6) is higher than that for C2 (SEH=2.4), resulting in higher maximum char conversion (Fig. 5(a)). On the contrary, the inert solids inventory in the riser-combustor (Fig. 7(b)) is higher in C1 since the larger riser requires from higher solids inventory to compensate a given pressure drop.

The minimum of riser solids inventory reached in C1 is explained in Fig. 7(c). It is observed that for SEH below 1.4 there is a net decrease in pressure drop in the gasifier side (the decrease in the pressure drop of the LLS SC is faster than the increase in the pressure drop in the gasifier) which is compensated in the riser (Fig. 7(d)) by decreasing the solids inventory. For SEH above 1.6 the opposite behavior is observed, and the riser needs to allocate more solids to compensate the increase in pressure drop in the gasification unit. In a similar way the solids inventory profile for C2 can be related with the pressure profiles in Fig. 7(c,d). On the contrary, it is observed that for C2 the pressure drop profile in the LLS SC is not linear but following a similar trend to that of the gasifier (for SEH≤2.1), resulting in a much constant solids inventory in the riser. The explanation is in Fig. 7(e) where it can be seen that under C2 the solids velocity (hence, solids circulation) in the LLS is constant for all the SEH range and, a net flow of gas countercurrent to solids is fed for controlling the pressure drop. On the contrary, under C1 the control of the pressure drop is given by the change of the solids velocity against a stagnant gas (which results in a linear decrease in the LLS SC pressure drop) minimizing the gas fed to the SC to that needed to avoid the gas dragging from the gasifier.

4.3. Sensitivity analysis

A sensitivity analysis was made to assess the flexibility of the system under changes in the char reactivity, the gasification temperature, the HMS temperature and the throughput of biomass, taking C1 as a reference. The maximum SEH and char conversion reached in the gasification unit for the maximum pressure drop of 200 mbar set in the study, are assessed while varying one parameter and keeping the rest as in the reference case (Table 2).

4.3.1. Char reactivity

The flexibility of the SDFBG for processing biomasses with different reactivities is assessed in Fig. 8(a) by a factor multiplying the reactivity in the reference case [29], as well as other reactivities for wood char from literature [30,31].

As expected, increasing the reactivity leads to a reduction of the solids inventory required in the gasifier for a given SEH (lower char residence time required to convert the char). In that way the maximum SEH can be increased a 14% over that of the reference case if the reactivity is doubled, while it decreases a 22% if the reactivity is halved. This implies maximum char conversions of 88 and 65%, respectively, compared to 79% of the reference case.

Results from Fig. 8(a) show that the proposed system is robust enough to allow some room for processing materials with different reactivities. The kinetics obtained by Barrio at al. [30] for birch char leads to a reactivity below the half of that of the reference case, and still allows char conversions over 60% and SEH of 1.9 MJ/$kg_{bio,daf}$. Reaction rates far below this [32,33] would require from a redesign of the system. Note that we have assumed one single stage unit for the gasifier, but there are other solutions such as using a staged fluidized bed or the use of an external catalyst. The former measure increases the char conversion for a given mass inventory (and temperature) since the number of stages allows approaching the solids circulation to the plug flow. The use of catalyst to reduce the required residence time has been verified for coal gasification in fluidized bed with various alkaline oxides and carbonates [34]. Although demonstration at large scale is still uncertain, catalytic gasification is already offered in the market as bluegas™ catalytic hydromethanation process by Greatpoint Energy [35] and extensive research is being carried out, for instance to produce methane from biomass [36]. Therefore, the combination of SDFBG with catalytic gasification seems to be a promising technology to explore.

4.3.2. Gasification temperature

As shown in Fig. 8(b), increasing the gasification temperature to 895 °C allows increasing the maximum SEH in a 24% while rising the maximum char conversion from 79 to 87% due to the increase in the char gasification rate. However, although not shown in Fig. 8(b), the benefit of increasing the gasification temperature disappears as the SEH is lowered and more heat is required from the combustor, since the internal solids circulation becomes very high due to the low driving force of temperature between the gasification and combustion units. This huge circulation of solids leads to lower residence time of char for a given solids inventory in the gasifier (Eq. (7)), i.e., the residence time limits and it overcomes the increased reaction rate resulting in a lower char conversion (compared to that obtained at lower gasification
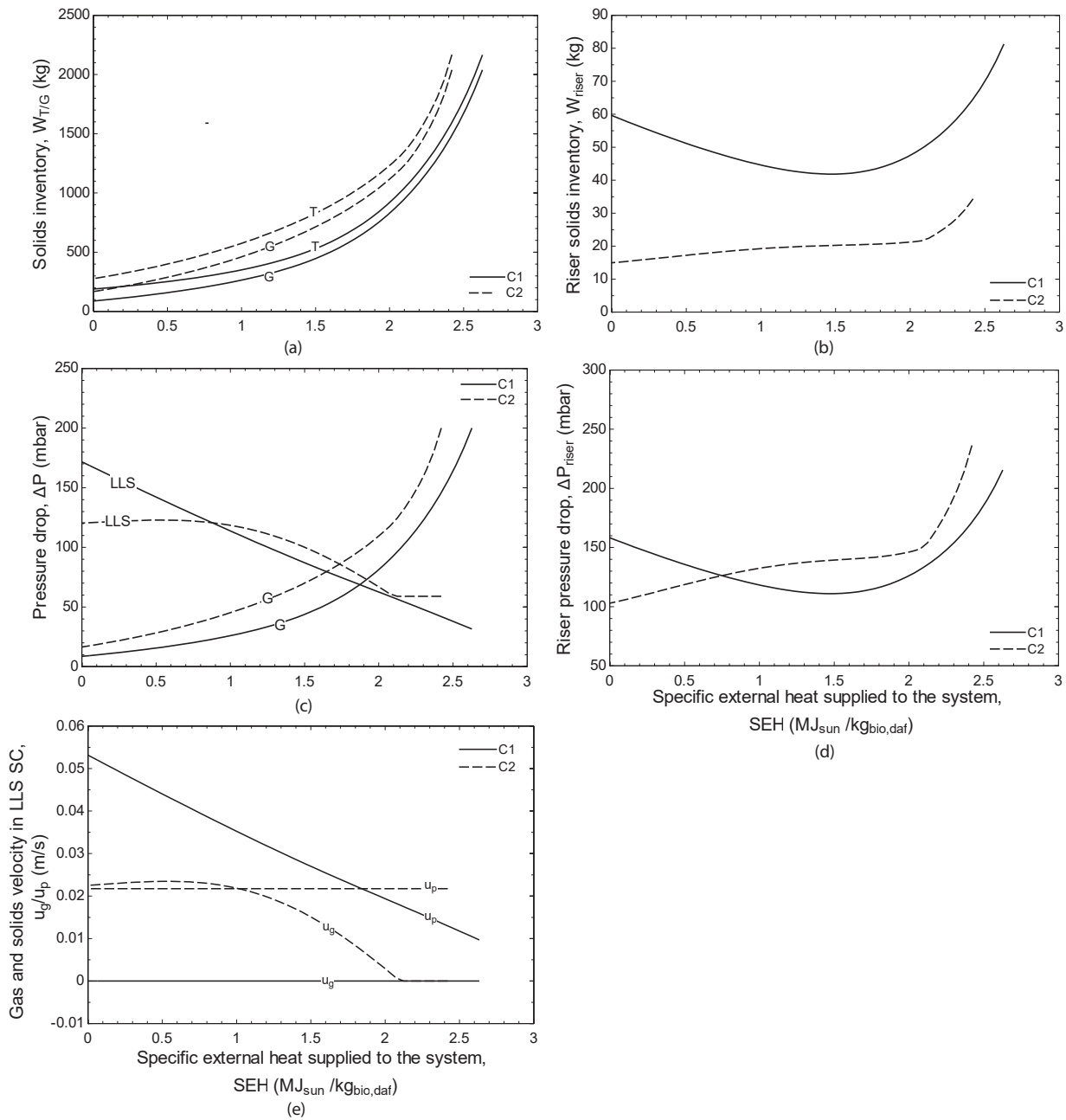
Fig. 7. Total solids inventory in the system, T, and in the gasification unit, G (a), inventory of solids in the riser-combustor (b), pressure drop of the gasifier, G, and the supply chamber of the LLS, LLS (c), pressure drop of the riser (d) and gas and solids actual velocity in the LLS SC (e), as a function of SEH in SDFBGs for C1 and C2 (Fig. 2) and operating conditions of Table 2.

temperature).

The opposite behavior is found in Fig. 8(b) when decreasing the gasification temperature to 805 °C, the kinetic rate is lowered and a higher residence time is required for converting the char (i.e., a lower maximum char conversion is reached in the gasifier for the 200 mbar pressure drop). On the contrary, at low SEH loads, a much higher char conversion would be reached (compared to that at T_G=895 °C) due to the reduction of the internal solids circulation.

Therefore, for C1, an optimal operation by modifying the gasification temperature is: increasing the gasification temperature at high allothermal operation to maximize the SEH input while decreasing it as the load of SEH is reduced to minimize the internal (gasifier-combustor) solids circulation. Additional aspects as tar conversion limitations need to be considered when selecting the gasifier range of temperature. As discussed above, the operation at constant temperature is generally safer

and this could prevail over other performance considerations.

4.3.3. Temperature of the solids from the HMS

Fig. 8(c) shows that increasing the temperature of the HMS from 950 to 1000 °C the maximum SEH introduced to the system is increased a 7% over that of the reference case, resulting in a higher maximum char conversion in the gasifier (84% compared to 79% of the reference case). For a given SEH, if the temperature of the HMS is increased, the external solids circulation is lowered (higher driven force of temperature between the HMS and the gasifier). This implies (as follows by Eq. (7)) that, for the given gasification unit operating at the maximum pressure load (200 mbar), the residence time of the char is higher leading to a higher char conversion.
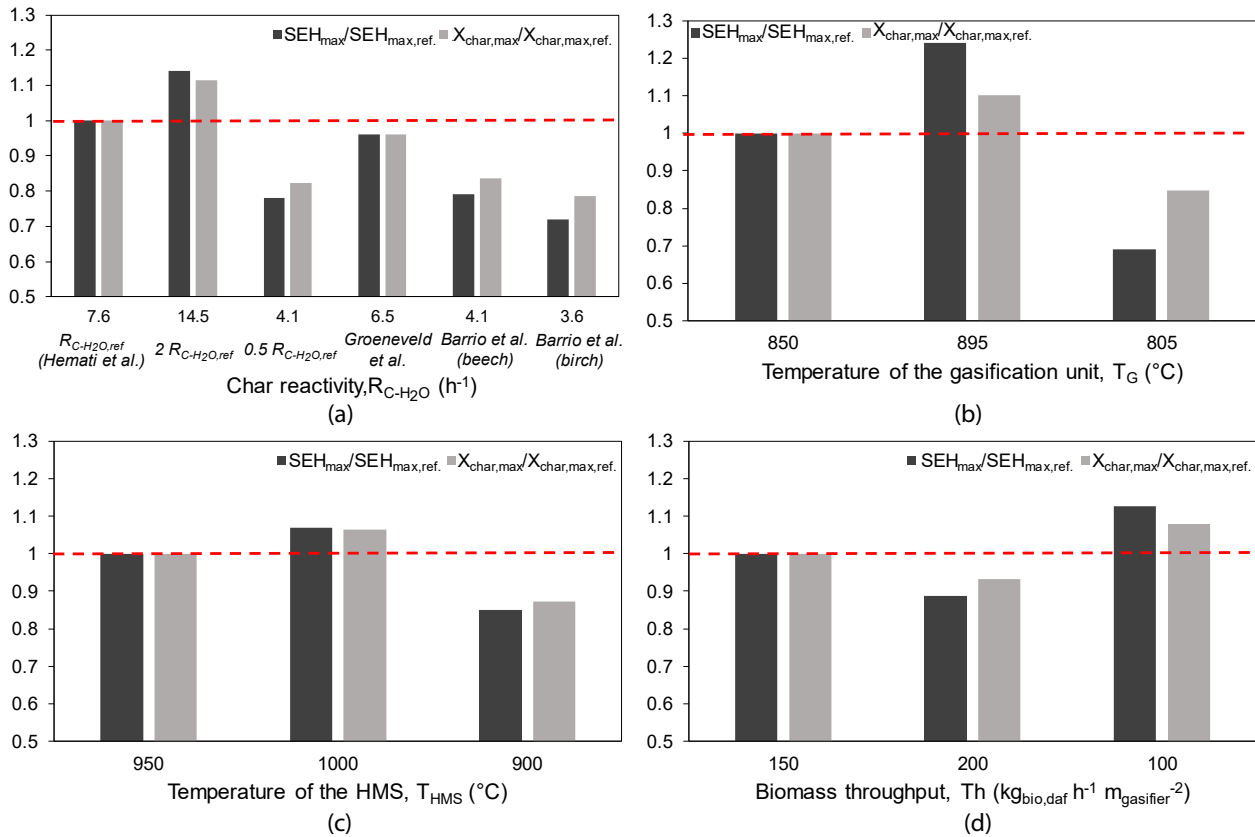
Fig. 8. Relative maximum SEH, SEH$_{max}$/SEH$_{max,ref}$ (2.63 MJ/kg$_{bio,daf}$) and relative maximum char conversion in the gasifier, X$_{char,max}$/X$_{char,max,ref}$ (0.79) for C1, for the maximum pressure drop set for the gasification unit (200 mbar) for: (a) the char reactivity used in the reference case (R$_{C-H2O,ref}$, Hemati et al. [29]), parametric variations on this, 2 R$_{C-H2O,ref}$ and 0.5 R$_{C-H2O,ref}$, and other kinetic rates (Barrio et al. [30], Groeneveld et al. [31]), reactivity is defined as: R$_{C-H2O}$ = 1/(1-x$_{char}$)dx$_{char}$/dt; (b) different gasification temperatures; (c) different temperatures of the HMS and (d) different throughput of biomass.

4.3.4. Throughput of biomass

The flexibility of the system for operating under different throughputs of biomasses is assessed in Fig. 8(d). As expected, the higher the throughput of biomass, the lower the maximum SEH introduced to the system compared to that of the reference case (a decrease of 11% is observed when increasing the throughput from 150 to 200 kg h^{-1} m$_{gasifier}^{-2}$), due to the lower residence time of the char in the gasifier (for a constant maximum pressure drop of 200 mbar). As a result, a lower maximum char conversion is attained for higher throughput. However, note that, although the maximum SEH is lower for higher biomass throughput, the net input of solar energy is higher (an increase of 70 MJ is obtained when increasing the throughput from 150 to 200). Therefore, depending on the availability of both, biomass and solar resource, and the demand of product gas, the throughput of biomass can be adapted to optimize the operation.

5. Conclusions

A new DFBG for carrying out the steam gasification of biomass assisted by heat carriers (heated in a solar particle receiver) was designed. A model was developed to take into account both, thermochemical and fluid-dynamics challenges. It calculates the char conversion in the gasifier and syngas composition, the solids circulation, the gas flowrate needed in the combustor, the inventory of solids and the pressures and solids distribution around the system for given operating conditions.

Geometric relations are given for the solar DFBG under two different configurations for external solids circulation removal (C1, from the gasifier and C2, from the combustor). The geometric relations adopted can be slightly varied but the trends and main conclusions will stand.

Special attention needs to be paid (for designing and scaling purposes) when modeling the riser, since the solids entrainment couples the thermochemistry and the fluid-dynamics of the process and, semi-empirical entrainment models as the one adopted in this study need to be carefully used.

The main results from the study are:

- The designed SDFBG allows the operation both, under autothermal and at high allothermal conditions, leading to char conversions in the gasifier from 15 to 80%.
- The configuration of the external solids circulation results in significant variations in the design and operation of the SDFBG due to the different patterns of solids circulation.
- For the operating conditions of the reference case, the maximum allowable SEH is 2.6 MJ/kg$_{bio,daf}$ for the SDFBG designed for operated under C1 and 2.4 MJ/kg$_{bio,daf}$ for that designed for operating under C2.
- Biomasses with char reactivities around the half of that used for designing the SDFBG can be processed leading to a maximum char conversion in the gasifier of 65% (SEH=2.1 MJ/kg$_{bio,daf}$) under C1
- The operation for C1 can be optimized by changing the temperature in the gasification unit: increasing it at the high range of SEH, while decreasing it as the SEH is reduced.
- Increasing the temperature of the hot solids material storage from 950 to 1000 °C enhances a 7% the maximum SEH (5% of increase in the char conversion) under C1.
- The throughput of biomass can be adapted to optimize the operation of the SDFBG according to the availability of both, biomass and solar resources.

Overall, the results show that the proposed SDFBG presents huge potential for being scaled-up taking the most of current state-of-the-art technologies of DFBG after some modifications, mainly: a wider gasifier unit, a narrower riser-combustor and a dedicated lower loop seal for adapting the operation to changes in external heat loads. Moreover, the combination of solar DFBG with catalytic gasification seems to be a promising technology to provide even further benefits.

CRediT authorship contribution statement

M. Suárez-Almeida: Investigation, Conceptualization, Methodology, Formal analysis, Writing – original draft, Visualization. **A. Gómez-Barea:** Conceptualization, Methodology, Resources, Funding acquisition, Project administration, Supervision, Writing – review & editing. **J. Salinero:** Writing – review & editing.

Declaration of Competing Interest

The authors declare the following financial interests/personal relationships which may be considered as potential competing interests: Montserrat Suárez Almeida has patent *Módulo de lecho fluidizado dual para gasificación de biomasa y residuos con energía solar e instalación y método de operación asociado* pending to Universidad de Sevilla. Alberto Gómez Barea has patent *Módulo de lecho fluidizado dual para gasificación de biomasa y residuos con energía solar e instalación y método de operación asociado* pending to Universidad de Sevilla.

Data availability

No data was used for the research described in the article.

Acknowledgements

References

[1] Kodama T. High-temperature solar chemistry for converting solar heat to chemical fuels. Prog Energy Combust Sci 2003;29:567–97. https://doi.org/10.1016/S0360-1285(03)00059-5.

[2] Nzihou A, Flamant G, Stanmore B. Synthetic fuels from biomass using concentrated solar energy - A review. Energy 2012;42:121–31. https://doi.org/10.1016/j.energy.2012.03.077.

[3] Puig-Arnavat M, Tora EA, Bruno JC, Coronas A. State of the art on reactor designs for solar gasification of carbonaceous feedstock. Sol Energy 2013;97:67–84. https://doi.org/10.1016/j.solener.2013.08.001.

[4] Abanades S, Rodat S, Boujjat H. Solar thermochemical green fuels production: A review of biomass pyro-gasification, solar reactor concepts and modelling methods. Energies 2021;14. https://doi.org/10.3390/en14051494.

[5] Guo P, Van Eyk PJ, Saw WL, Ashman PJ, Nathan GJ, Stechel EB. Performance assessment of Fischer-Tropsch liquid fuels production by solar hybridized dual fluidized bed gasification of lignite. Energy Fuel 2015;29:2738–51. https://doi.org/10.1021/acs.energyfuels.5b00007.

[6] Guo P, Saw WL, Van Eyk PJ, Stechel EB, Ashman PJ, Nathan GJ. System optimization for Fischer-Tropsch liquid fuels production via solar hybridized dual fluidized bed gasification of solid fuels. Energy Fuel 2017;31:2033–43. https://doi.org/10.1021/acs.energyfuels.6b01755.

[7] Gómez-Barea A, Suárez-Almeida M, Ghoniem A. Analysis of fluidized bed gasification of biomass assisted by solar-heated particles. Biomass Convers Biorefinery 2021;11:143–58. https://doi.org/10.1007/s13399-020-00865-0.

[8] Suárez-Almeida M, Gómez-Barea A, Ghoniem AF, Pfeifer C. Solar gasification of biomass in a dual fluidized bed. Chem Eng J 2021;406. https://doi.org/10.1016/j.cej.2020.126665.

[9] Corella J, Toledo JM, Molina G. A review on dual fluidized-bed biomass gasifiers. Ind Eng Chem Res 2007;46:6831–9. https://doi.org/10.1021/ie0705507.

[10] Suárez-Almeida M, Gómez-Barea A, Pfeifer C, Leckner B. Fluid dynamic analysis of dual fluidized bed gasifier for solar applications. Powder Technol 2021;390:482–95. https://doi.org/10.1016/j.powtec.2021.05.032.

[11] Turn S, Kinoshita C, Zhang Z, Ishimura D, Zhou J. An experimental investigation of hydrogen production from biomass gasification. Int J Hydrogen Energy 1998;23:641–8. https://doi.org/10.1016/s0360-3199(97)00118-3.

[12] Gómez-Barea A, Leckner B. Estimation of gas composition and char conversion in a fluidized bed biomass gasifier. Fuel 2013;107:419–31. https://doi.org/10.1016/j.fuel.2012.09.084.

[13] Lundberg L, Pallarès D, Thunman H. Upscaling effects on char conversion in dual fluidized bed gasification. Energy Fuel 2018;32:5933–43. https://doi.org/10.1021/acs.energyfuels.8b00088.

[14] Johnsson F, Andersson S, Leckner B. Expansion of a freely bubbling fluidized bed. Powder Technol 1991;68:117–23. https://doi.org/10.1016/0032-5910(91)80118-3.

[15] Suárez-Almeida M, Gómez-Barea A. Fluid-dynamics of a loop seal: an experimental study. 24 Th Fluid. Bed Convers. Conf., Gothenburg. 2022.

[16] Suárez-Almeida M, Gómez-Barea A. On the comprehension of the gas split in loop seal devices. Powder Technol 2022:408. https://doi.org/10.1016/j.powtec.2022.117777.

[17] Kunii D, Levenspiel O. Fluidization engineering. 2nd ed. Stoneham: Butterworth-Heinemann; 1992. 10.1016/b978-0-7506-9236-6.50001-9.

[18] Lewis WK, Gilliland ER, Lang PM. Entrainment from fluidized beds. Chem Eng Prog Symp Ser 1962;58–65.

[19] Morin M, Raynal L, Karri SBR, Cocco R. Effect of solid loading and inlet aspect ratio on cyclone efficiency and pressure drop: Experimental study and CFD simulations. Powder Technol 2021;377:174–85. https://doi.org/10.1016/j.powtec.2020.08.052.

[20] Colakyan M, Levenspiel O. Elutriation from fluidized beds. Powder Technol 1984;38:223–32. https://doi.org/10.1016/0032-5910(84)85005-6.

[21] Shepherd CB, Lapple CE. Flow Pattern and Pressure Drop in Cyclone Dust Collectors: Cyclone without Inlet Vane. Ind Eng Chem 1940;32:1246–8. https://doi.org/10.1021/ie50369a042.

[22] Grace J. Handbook of multiphase systems. Washington, D.C.,: Hemisphere Publishing; 1982.

[23] Haider A, Levenspiel O. Drag coefficient and terminal velocity of spherical and nonspherical particles. Powder Technol 1989;58:63–70. https://doi.org/10.1021/ie50688a011.

[24] Hofbauer H, Rauch R. Stoichiometric water consumption of steam gasification by the FICFB-gasification process. Prog Thermochem Biomass Convers 2008. https://doi.org/10.1002/9780470694954.ch14.

[25] Karl J, Pröll T. Steam gasification of biomass in dual fluidized bed gasifiers: A review. Renew Sustain Energy Rev 2018. https://doi.org/10.1016/j.rser.2018.09.010.

[26] Pfeifer C, Schmid J, Pröll T, Hofbauer H. Next generation biomass gasifier. 19th Eur. Biomass Conf. Exhib. Berlin, Ger.. 2011.

[27] T. Pröll, C. Aichernig, R. Rauch, H. Hofbauer, Performance characteristics of an 8 MWth combined heat and power plant, in: 12th Int. Conf. Fluid. - New Horizons Fluid. Eng., 2007. https://doi.org/10.2202/1542-6580.1398.

[28] M. Suárez-Almeida, A. Gómez-Barea, Módulo de lecho fluidizado dual para gasificación de biomasa y residuos con energía solar e instalación y método de operación asociado, ES1650.153, 2022.

[29] Hemati M, Laguerie C. Détermination de la cinétique de vapogazéification de charbon de bois en thermobalance. Entropie 1988;142:29–40.

[30] Barrio M, Gøbel B, Rimes H, Henriksen U, Hustad JE, Sørensen LH. Steam gasification of wood char and the effect of hydrogen inhibition on the chemical kinetics. Prog Thermochem Biomass Convers 2008:32–46. https://doi.org/10.1002/9780470694954.ch2.

[31] Groeneveld MJ, van Swaaij WPM. 39 Gasification of char particles with CO2 AND H2O. Chem Eng Sci 1980;35:307–13. https://doi.org/10.1016/0009-2509(80)80101-1.

[32] Kojima T, Assavadakorn P, Furusawa T. Measurement and evaluation of gasification kinetics of sawdust char with steam in an experimental fluidized bed. Fuel Process Technol 1993;36:201–7. https://doi.org/10.1016/0378-3820(93)90028-3.

[33] Bhat A, Ram Bheemarasetti JV, Rajeswara Rao T. Kinetics of rice husk char gasification. Energy Convers Manag 2001;42:2061–9. https://doi.org/10.1016/S0196-8904(00)00173-4.

[34] Hirsch RL, Gallagher JE, Lessard RR, Wesselhoft RD. Catalytic coal gasification: An emerging technology. Science (80-.) 1982;215:121–7. https://doi.org/10.1126/science.215.4529.121.

[35] NETL, Great Point Energy, Gasifipedia. (2017). https://www.netl.doe.gov/research/coal/energy-systems/gasification/gasifipedia/gpe (accessed February 11, 2022).

[36] Nanou P. Biomass gasification for the production of methane. Univ Twente 2013:173. http://purl.org/utwente/doi/10.3990/1.9789036535434.